PCCP

ROYAL SOCIETY OF CHEMISTRY

PAPER

Published on 13 July 2026

Cite this: *Phys. Chem. Chem. Phys.*, 2026, **28**, 19314

Vibrational oscillations in transient absorption spectra during singlet fission in a butyl-substituted bis(thienyl)-diketopyrrolopyrrole with efficient singlet fission

Miroslav Menšík, *[a] Petr Toman, [a] Igor Rončević, [b] Alexandr Zaykov, [c] Petr Kužel, [d] Jan Pokorný, [d] David Rais, [a] Muhammed A. Thottappali [a] and Jiří Pfleger [a]

Received 20th March 2026,
Accepted 11th July 2026

DOI: 10.1039/d6cp01025c

rsc.li/pccp

By analyzing previously reported transient absorption spectra of thin films of diketopyrrolopyrroles carrying *n*-hexyl, *n*-butyl, or 2-(adamant-1-yl)ethyl substituents, we found that the efficient singlet fission is accompanied by small but observable oscillations on the ps time scale. Specifically, clearly resolved vibrational oscillations with a period of 1.6 ps were observed in the time course of the transient absorption of thin films of *N*,*N*′-di-*n*-butyl-2,5-dihydro-3,6-bis-2-thienylpyrrolo[3,4-*c*]pyrrole-1,4-dione prepared by spin-casting, with a singlet fission yield approaching 160%. Here we show that these oscillations are formed by a population exchange between singlet and triplet-pair excitations, which is controlled by the inter-molecular vibrations of adjacent molecules in a centrosymmetric crystal configuration. Due to a very broad spectral distribution of these low-frequency vibrational modes developed after the photoexcitation, the probability of the conical intersection of the potential energy surfaces related to singlet and triplet-pair states is efficiently increased. The singlet and triplet states population exchange facilitated by coherently excited vibrations near the conical intersection also changes the transition dipole moments seen in the optical time-resolved pump–probe experiment. It was shown that these oscillations decay within the initial *ca.* 10 ps after photoexcitation, while on a timescale of 90 ps, the transient spectra gradually evolve into a long-lived component, formed exclusively by the triplet states.

1. Introduction

Singlet fission (SF), representing the conversion of a singlet exciton into a triplet-pair state, offers an elegant mechanism for improving the efficiency of light-harvesting devices. To be competitive, the process of SF must be faster than any other competing relaxation or deexcitation processes. This has motivated many time-resolved optical studies of phenomena immediately following the electronic excitation. Several such studies on molecular organic solids have reported damped oscillations in the intensity of transient optical absorption with periods on the order of 100 fs up to picoseconds lasting up to tens of periods after an initial short-pulse excitation.[1–15] Recently, it was proved that explicit coupling of electronic states to inter-molecular (Peierls) vibrational modes accelerates the SF.[16]

In our previous study,[9] we examined the SF in thin films of derivatives of diketopyrrolopyrroles (TDPPs) carrying *n*-hexyl, *n*-butyl, or 2-(adamant-1-yl)ethyl substituents using transient optical absorption (TA) spectroscopy. They were prepared in the form of thin films using spin-casting (SC), vapor deposition (VD) or vapor deposition with subsequent solvent annealing (VD-SA). TA spectra could be fitted by evolution associated spectra within a two- or three-component model with the corresponding decay rates k_i (see Table S1 in the SI). In several cases, an initial fast decay was also observed and expressed with the rate constant k_1, assigned to a hot singlet excited state annihilation. The rate constant k_2 is composed of a combination of two processes, namely the internal conversion k_{ic} and the triplet state formation $k_{SF} = \frac{\Phi_T}{2} \cdot k_2$, where Φ_T denotes the quantum yield of the triplet state formation (and thus $\frac{\Phi_T}{2}$ is

[a] *Department of Polymers for Electronics and Photonics, Institute of Macromolecular Chemistry CAS, Heyrovského nám. 1888/2, 162 06 Prague, Czech Republic. E-mail: mensik@imc.cas.cz*
[b] *Department of Chemistry, The University of Manchester, Oxford Road, Manchester M13 9PL, UK*
[c] *Institute of Organic Chemistry and Biochemistry of the CAS, Flemingovo nám. 542/2, 160 00 Prague, Czech Republic*
[d] *Institute of Physics CAS, Na Slovance 2, 182 00 Prague, Czech Republic*

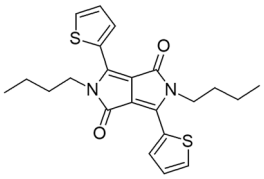

Bu-TDPP

Scheme 1 Chemical structure of *N*,*N*′-di-*n*-butyl-2,5-dihydro-3,6-bis-2-thienylpyrrolo[3,4-*c*]pyrrole-1,4-dione (Bu-TDPP).

equal to the efficiency of the formation of triplet pair states). The rate constant k_3 determines the triplet state lifetime. We noted that when a non-zero yield of the triplets was found, the lifetime ${k_3}^{-1}$ of the triplet state was always longer than 10 ns. In this study, we revisited our previously measured data and found that when the quantum yield of the triplet states was higher than 100%, and the excitation energy thus spread over two molecules, clearly resolved oscillations were present in TA shortly after photoexcitation (see Table S1 in the SI). For cases when the triplet yield was lower, less pronounced oscillations were found.[9] The aim of this study is to find a correlation between the oscillations in TA spectra, which occur in the ps time-scale, and the SF yield, determined from the long-time asymptote on the ns scale. In doing this, we made a detailed analysis of such oscillations in the TA spectra of spin-cast thin solid films of *N*,*N*′-di-*n*-butyl-2,5-dihydro-3,6-bis-2-thienylpyrrolo-[3,4-*c*]pyrrole-1,4-dione (SC Bu-TDPP, Scheme 1), where the highest triplet yield of ∼160% was found,[9] utilizing the method of Carmichael and Haug.[17]

In our previous report,[9] we presumed that the excited state is a momentum-dependent exciton with Davydov energy level splitting due to the presence of four molecules in the unit cell, and that SF proceeds *via* intermediate charge transfer states. This kind of model implicitly assumed a high degree of crystallinity. In this study, we critically revisit these assumptions for SC Bu-TDPP thin films, which showed high SF yield despite their lower crystallinity compared to other samples (see the XRD data in Fig. S38–S40 in ref. 9). We explain the origin of the above-mentioned oscillations in TA as a consequence of the population exchange between singlet and triplet-pair states.

One can note that the frequency of the observed oscillations (∼20 cm^{-1}) is on the same order of magnitude as the low-frequency inter-molecular vibrational modes. These modes can be excited by at least two processes: (i) direct excitations by photons with a sufficient excess of energy to induce these vibrations, and (ii) by an explicit dependence of the electronic transition dipole moments of the ground state absorption on the instant amplitude of inter-molecular vibrations, which induces a non-equilibrium vibrational distribution after the photoexcitation.

The transition dipole moment between the excited electronic states observed by the probe pulses in TA spectroscopy could oscillate with the inter-molecular mode frequency. In this case, the magnitude of oscillations observed in the TA spectra would be determined by the degree of modulation of the electronic wave function in the excited-state manifold by the inter-molecular vibrations, *i.e.*, by the electron-vibrational coupling. The observed decay time of these oscillations (∼10 ps) appears to support this hypothesis, as it is in agreement with the observed rates of vibrational cooling.[18,19]

As shown in our previous study on Bu-TDPP,[9] adjacent molecules in the unit cell are in a J-aggregated centrosymmetric configuration (*i.e.*, with mutually oppositely oriented transition dipole moments on adjacent molecules). The state which is directly excited by the pump pulse (see eqn (S.II.4) in the SI), may be written as a singlet excitation spanned on a dimer

$$|\mathrm{S}^-\rangle = \frac{1}{\sqrt{2}}(|\mathrm{S}_1,\mathrm{S}_0\rangle - |\mathrm{S}_0,\mathrm{S}_1\rangle), \quad (1)$$

while the other possible excitonic configuration

$$|\mathrm{S}^+\rangle = \frac{1}{\sqrt{2}}(|\mathrm{S}_1,\mathrm{S}_0\rangle + |\mathrm{S}_0,\mathrm{S}_1\rangle), \quad (2)$$

cannot be directly excited by the pump pulse, as the corresponding transition dipole moment is zero (see eqn (S.II.4) in the SI). Since it is also much higher in energy, it can be ignored. The state $|\mathrm{S}^-\rangle$ can undergo a SF yielding a singlet biexciton $|\mathrm{T}_1,\mathrm{T}\rangle$ as an intermediate state before the dissociation into two independent triplets. This biexciton is composed of two entangled triplet excitons located on both adjacent molecules. In materials, where the SF proceeds efficiently, the initial singlet exciton and the singlet biexciton are typically nearly degenerate and the amount of released vibrational energy is small.

The $|\mathrm{S}^-\rangle$ exciton and the $|\mathrm{T}_1,\mathrm{T}_1\rangle$ biexciton may mix together to give two adiabatic states

$$|\varphi^+\rangle = \cos(\alpha)|\mathrm{S}^-\rangle + \sin(\alpha)|\mathrm{T}_1,\mathrm{T}_1\rangle \quad (3)$$

$$|\varphi^-\rangle = \cos(\alpha)|\mathrm{S}^-\rangle - \sin(\alpha)|\mathrm{T}_1,\mathrm{T}_1\rangle \quad (4)$$

with the mixing angle α given by

$$\tan(2\alpha) = \frac{2\langle \mathrm{S}^-|H_{\mathrm{int}}|\mathrm{T}_1,\mathrm{T}_1\rangle}{\Delta\varepsilon}, \quad (5)$$

where H_{int} is the interaction Hamiltonian and $\Delta\varepsilon$ is the energy difference between $|\mathrm{S}^-\rangle$ and $|\mathrm{T}_1,\mathrm{T}_1\rangle$.

The excitation with a ∼100 fs pump pulse causes a transfer of a fraction p of the ground state population into the excited state manifold with a lifetime that is much longer than the period of the observed oscillations. This fraction p of excited molecules induces a partial bleach of the ground state absorption, *i.e.*, $|\mathrm{S}_0,\mathrm{S}_0\rangle \rightarrow |\mathrm{S}^-\rangle$, seen by the second (probe) beam that enters the system after a time delay t. This bleach appears as a negative signal in the differential TA spectra, because they show the difference between the instant time-dependent absorbance seen by the probe and the steady-state absorbance. On the other hand, these excited molecules will also induce new transitions from the bottom adiabatic state $|\varphi^+\rangle$ to a manifold of higher excited states $|\varphi_n\rangle$, yielding a positive contribution to the differential TA spectra. Among these transitions, $|\mathrm{S}^-\rangle \rightarrow |\mathrm{S}_1,\mathrm{S}_1\rangle$ and $|\mathrm{T}_1,\mathrm{T}_1\rangle \rightarrow |\mathrm{T}_1,\mathrm{T}_x\rangle$, the latter being very similar to

intramolecular transitions $|T_1\rangle \rightarrow |T_x\rangle$, are the most characteristic ones. These two types of transitions contribute differently to the excited state absorption (ESA) spectra. As both the transition frequency and the width of the intermolecular vibration distribution will periodically oscillate, we expect both $\Delta\varepsilon$ and $\langle S^-|H_{int}|T_1,T_1\rangle$ to change in time accordingly. It will induce a periodic change in the mixing angle $\alpha = \alpha(t)$ and in the ESA corresponding to the electronic transition $|S^-\rangle \rightarrow |S_1,S_1\rangle$ or $|T_1,T_1\rangle \rightarrow |T_1,T_x\rangle$. For the respective transition dipole moments of these processes we find $|\langle S_1,S_1|d|\varphi^+(\alpha)\rangle|^2 = \cos^2(\alpha)|\langle S_1,S_1|d|S^-\rangle|^2$ and $|\langle T_1,T_x|d|\varphi^+(\alpha)\rangle|^2 = \sin^2(\alpha)|\langle T_1,T_x|d|T_1,T_1\rangle|^2$. Through eqn (5), the value of the time-dependent mixing parameter $\langle S^-|H_{int}|T_1,T_1\rangle/\Delta\varepsilon$ explicitly controls the respective weights $\cos^2(\alpha)$ and $\sin^2(\alpha)$ of the ESA of the singlet and triplet-pair states. Thus, we can expect that both contributions to ESA will be periodically modulated by an intermolecular vibration mode, and they will be mutually phase-shifted by π.

These oscillations in TA can occur only in the coherent state of the system that occurs shortly after photoexcitation. Upon relaxation of the intermolecular mode, the oscillations will thermalize and consequently, the mixing parameter $\tan(2\alpha)$ becomes small and the irreversible SF process takes place.

The first goal of this work is to investigate whether the observed modulation of TA spectra by low-frequency vibrations is indeed due to the population exchange between the singlet exciton and singlet biexciton (triplet-pair), or to perturbations in the transition dipole moment of the singlet exciton caused by some other process, *e.g.*, the vibration-controlled momentum-dependent exciton band dispersion or the impulsive stimulated Raman scattering (ISRS).[20] We propose a SF model, in which the excited state is essentially delocalized just on a dimer formed by two strongly interacting molecules of the total four molecules in the elementary cell, and the SF is controlled by their inter-molecular oscillations.

The second goal of this study is to explain the mutual connection between the vibrationally driven oscillations in TA on the ps time scale and the irreversible triplet formation, which occurs during *ca.* 90 ps.

2. Results and discussion

For better clarity, we divide this part of the article into three sections:

In Section 2.1 we compare the ground state absorption of Bu-TDPP in thin films and in toluene solutions and show that the initial excitation cannot be substantially delocalized in space outside of the elementary cell composed of four molecules, while we found the Franck–Condon transitions corresponding to the intra-molecular mode of energy 0.18 eV. This mode also contributes to the high reorganization energy after the photoexcitation. We also identified clearly resolved oscillations with a period of 1.6 ps in the TA spectra. In Section 2.2, we identify possible low-frequency inter-molecular modes by means of quantum chemical calculations, THz and Raman spectroscopies. In Section 2.3, we discuss three possible mechanisms that could explain the vibrational modulation of TA spectra: (i) vibrationally controlled population exchange between S and TT states, (ii) vibrationally driven modulation of the transition dipole moments involved in the SF process, and (iii) the impulsive stimulated Raman scattering (ISRS) process. We also explain the interconnection between short-term oscillations in the TA spectra and the irreversible transition to the triplet pair state at longer times.

2.1. Analysis of previous TA measurements

Fig. 1 compiles the most important experimental results of Bu-TDPP in SC thin films shown in ref. 9. In Fig. 1a, the differential TA spectrum is compared to the steady-state absorption. As the wavelength of the pump pulse was 465 nm, we limit our analysis of the differential TA spectrum to wavelengths longer than 470 nm. In the studied time interval, we can observe the formation of two sharp negative minima at 530 and 580 nm, which match the two maxima of equal intensity of the steady-state absorption at wavelengths of 528 and 572 nm found in ref. 9, corresponding to energies of 2.17 eV and 2.35 eV, respectively. Hence, they can be assigned to the ground state bleach (GSB, cyan curve in Fig. 1a). We also note a less pronounced shoulder in the steady-state absorption spectra around 490 nm (2.53 eV). All three peaks are equally separated by 0.18 eV. Very similar steady-state absorption spectral features were also found in the toluene solution of Bu-TDPP[9] and, hence, they can be assigned to the vertical intramolecular vibronic Franck–Condon (FC) transitions $|g,0\rangle \rightarrow |S_1,0\rangle$, $|g,0\rangle \rightarrow |S_1,1\rangle$, and $|g,0\rangle \rightarrow |S_1,2\rangle$, respectively. Their relative intensities were found to be *ca.* 1.0, 1.0, and 0.5. Considering that the intensities of the FC peaks are related to the Huang–Rhys factor S following the equation $|\langle 0|n\rangle|^2 = \frac{S^n}{n!}e^{-S}$, we obtained the Huang–Rhys factor $S \approx 1$. With the vibrational energy quantum $\hbar\Omega$ = 0.18 eV,[9] we can then obtain the reorganization energy of this vibrational mode of the molecule upon photoexcitation $\hbar\Omega S \approx 0.18$ eV. Contributions from other intramolecular modes can make the total reorganization energy even higher. Due to the high reorganization energy and simultaneously high Huang–Rhys factor S, the excited state could be dressed by this mode, supporting thus the excited state localization.

The pronounced localization of the excitations in SC films is consistent with their partially disordered structure (less resolved crystallinity in the XRD diffractograms in Fig. S38–S40 in ref. 9) that causes the values of excitonic transfer integrals based on the dipole–dipole interaction between adjacent molecules to be distributed in energy. In fact, the similarity of the steady-state absorption spectra of Bu-TDPP in SC thin films and solutions suggests that the excitation can be delocalized merely within the nearest molecules. Altogether, the better resolved FC peaks in the SC films are consistent with their lower crystallinity compared to other samples seen in XRD diffractograms.

On the other hand, in vapor deposited and solvent annealed thin films of Bu-TDPP, a spectral broadening of the intra-molecular

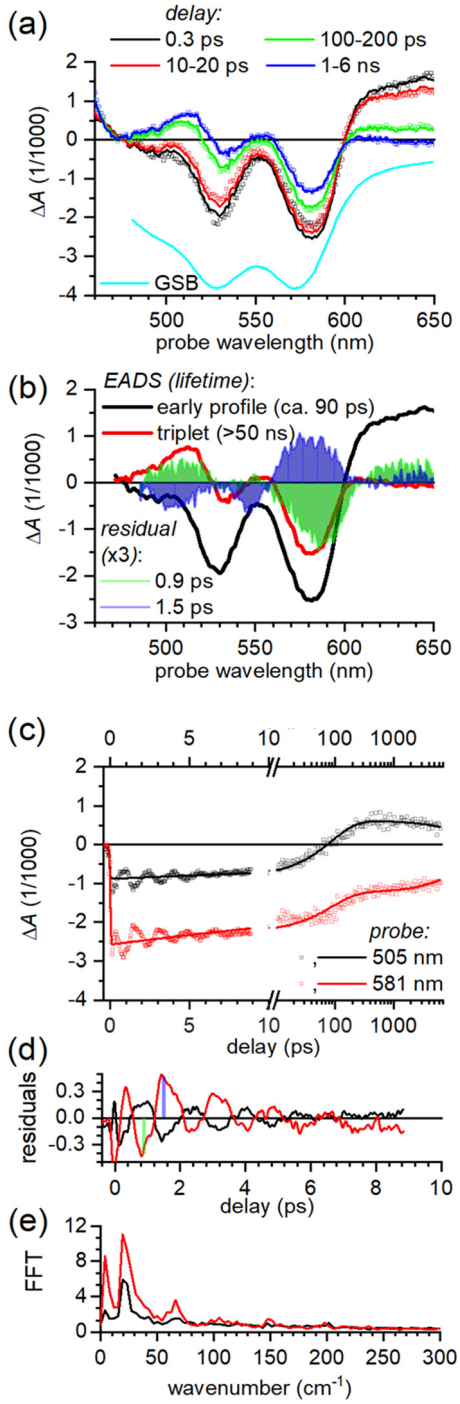

Fig. 1 Transient difference optical absorption of the Bu-TDPP SC thin films after photoexcitation by a laser pulse with a central wavelength of 450 nm: (a) representative TA spectra at various delay times (see the legend), compared to the ground state bleach calculated from the steady-state absorption and fraction of excited molecules (light blue), (b) time-invariant spectral profiles of the evolution-associated differential spectra, EADS, black and red curves) with respective lifetimes shown in the legend, compared to the oscillatory displacements around the mean values in the TA spectra at 0.9 ps and 1.5 ps (green and blue areas), (c) time course of TA recorded at 505 and 581 nm (black and red points) fitted by the time course calculated using eqn (6)–(8) (full lines), (d) residuals of the experimental time course of TA after subtraction of the fitted model curves shown in (c), and (e) the FFT spectrum of the residual signal shown in (d). Symbols in (a) and (c) denote experimental data, and the full lines indicate the best fits using the sequential EADS model. The blue and green vertical bars in (d) denote the temporal positions of the residual spectral profiles shown in (b) with the respective filling color.

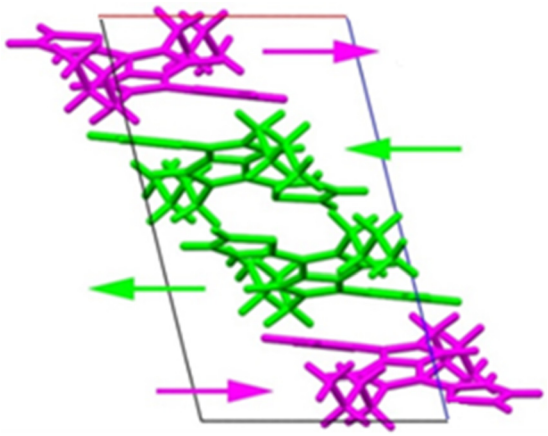

Fig. 2 Molecular translations involved in phonon mode 2. Molecules shown in purple move in the $+x$ (mode motion) direction, and those in green move in the $-x$ direction.

FC peaks was observed, corresponding to a partial exciton delocalization in the crystalline-like structure (Fig. 2 in ref. 9). This is manifested by a spectral peak broadening when going from the solution to the solid state, and also by the almost suppressed vibronic spectral features of the optical absorption spectra.

Besides the above-mentioned negative minima, we also find in Fig. 1 two broad regions of the positive difference absorbance. These bands come from the excited state absorption (ESA). The first one, found above 600 nm, was assigned to the absorption of S_1 states. After an initial relaxation within several ps, their early time hot population $c_1(t)$ evolves into a population of thermalized states $c_2(t)$, which further decays with a lifetime of about 90 ps (Fig. 1a). Concomitant with this decay, the ESA rises between 470 and 520 nm, corresponding to the formation of triplet states, as confirmed by its similarity to the spectrum of triplets generated in a sample containing a triplet sensitizer (Fig. S28 in the SI of ref. 9). Their lifetime exceeds the observation time window (6 ns) of the experiment. These triplets are generated by the SF process with a yield of 160%.[9]

After the initial relaxation of hot excitons, the evolution of the TA spectra can be successfully modelled by a two-level compartment model by a sum of two evolution associated differential spectra (EADS) as

$$\Delta A(\lambda, t) \approx \mathrm{EADS}(\lambda, \tau_2)c_2(t) + \mathrm{EADS}(\lambda, \tau_3)c_3(t). \quad (6)$$

With the populations $c_i(t)$ that satisfy the equations

$$\frac{\partial}{\partial t}c_2(t) = -{\tau_2}^{-1}c_2(t), \quad (7)$$

$$\frac{\partial}{\partial t}c_3(t) = {\tau_{\mathrm{SF}}}^{-1}c_2(t) - {\tau_3}^{-1}c_3(t). \quad (8)$$

Both populations $c_2(t)$ and $c_3(t)$ are hence assumed to undergo an exponential decay, the first one feeding the population of the second state $c_3(t)$. The respective EADS are shown in Fig. 1b, together with their corresponding lifetimes $\tau_2 = {k_2}^{-1} =$ 90 ps, $\tau_{\mathrm{SF}} = {k_{\mathrm{SF}}}^{-1}$ and $\tau_3 = 50$ ns, respectively.

The exponential-like process in eqn (7) indicates an absence of the bi-molecular annihilation that could occur due to collisions of delocalized excitons. This kind of bimolecular process would manifest itself as a power-law decay.[21–24] Assuming that the bi-molecular (singlet–singlet) annihilation does not occur during the initial *ca.* 90 ps, and taking into the account that the fraction of initially excited molecules in the SC Bu-TDPP thin film is about 10^{-2} (see Table S7 in the SI of ref. 9), we could conclude that the mean hopping time t_p of the excitation transfer between adjacent molecules must be longer than 1 ps. On the other hand, since the intramolecular relaxation typically occurs within approximately hundreds of femtoseconds, at 1 ps after photoexcitation, the excited states become already fully "dressed" by intramolecular vibrations with high reorganization energies. In this case, the probability of the formation of delocalized excitons is significantly reduced. Moreover, we can also prove that for typical values of the transfer integral J (based on transition dipole–dipole moments) between the nearest-neighbor molecules in an organic low-molecular-weight semiconductor, 0.1 eV $< J <$ 1 eV, the mean hopping time t_p of the Frenkel exciton between these molecules should be between 10 and 100 fs (see eqn (1)–(5) in the SI). This is another argument against the excitonic picture of the excited state. Therefore, a momentum-dependent excitonic picture does not seem likely.

The two-level model in eqn (6)–(8) explicitly excludes the formation of a population of intermediate charge transfer (CT) states. However, it does not exclude the coupling of S and TT states to CT states *via* the superexchange phenomenon (see Section II.S2 in the SI for a discussion of these effects). In fact, our quantum chemical calculations proved that the coupling of the excited state manifold to CT states interacting with low-frequency modes is possible (see Table S1 in the SI).

The residuals of the fit according to eqn (6)–(8) to the experimental data reveal short-lived oscillations with a period of 1.6 ps and a lifetime of about 10 ps (see Fig. 1b and c). The fast Fourier transformation (FFT) spectrum of these oscillations proved a significant component at 20 cm^{-1} (energy 2.5 meV) (Fig. 1e). We also note that the spectrum corresponding to the oscillations taken close to the time-domain minimum and maximum (green and blue curves in Fig. 1b) is very similar to the spectrum of the long-living component $c_3(t)$ formed by triplet states (*cf.* Fig. 1b). Then, we expect that the formation of oscillations is correlated with the SF process. We also note that the oscillatory components around 500 and 580 nm oscillate in mutually opposite phases. For a full 2D picture (wavelength, time) of the residuals see also Fig. S18 in the SI, where dominant regions of the antiphase oscillations are clearly resolved at regions centered at *ca.* 505 and 580 nm. We can also note a narrow band near *ca.* 550 nm, similar to that in Fig. 1b.

Clearly resolved periodic oscillations in the transient absorption spectra could originate, in principle, only in the electronic or vibrational coherences. Due to the very small energy of the oscillation energy quantum (2.5 meV), the electronic coherence can be excluded. This means that the electronic density matrix of the photoexcited system can be fully described only by the diagonal, *i.e.*, population terms, while the off-diagonal terms (so called "coherences") can be neglected.

2.2. Low frequency phonons

Before answering the question, which processes are responsible for the vibrational oscillations in the TA, we determine vibrational modes, which may contribute to the periodic oscillations with the period of 1.6 ps. In ref. 9, it was shown that SC thin films of Bu-TDPP crystalize in a $P2(1)/n$ monoclinic cell with parameters a = 9.48 Å, b = 13.80 Å, c = 16.48 Å, and $\alpha = 104.8^{\circ}$. There are four molecules in the unit cell (see Fig. S41 in the SI of ref. 9 illustrating the molecular packing as seen along major crystallographic axes). The formation of such a crystalline-like molecular structure strongly promotes the idea that the periodic oscillations in the TA spectrum come from the low frequency inter-molecular modes. Among such inter-molecular modes, we can find a class of modes around 20 cm^{-1}, or possibly at 10 cm^{-1} due to the influence of quadratic terms generating the components with the terms $\exp(\pm i2\omega t)$ (see below).

2.2.1. Quantum chemical calculations. Density functional theory calculations with periodic boundary conditions identified six lowest-lying phonon modes that roughly correspond to molecular translations, which alter the relative positions of the molecules in the unit cell but preserve their internal structure (Table 1 and Fig. 2). The calculated gamma-point frequencies of these modes are in the 10–30 cm^{-1} range (Table 1), making them viable candidates for modulating either (I) the population exchange or (II) the magnitude of the transition dipole moments. We carefully note that all six modes satisfy the symmetry against + and − inversion. Thus, their contribution to the TA spectra will be observed at the double frequency, leading to the terms $\exp(\pm i2\omega t)$.

2.2.2. THz spectroscopy. The THz spectra of the Bu-TDPP powder in a cuvette and in the form of a pressed pellet are shown in Fig. 3. The quality of the spectra obtained for the pressed pellet is much better and the morphology of this sample is also assumed to correspond better to that of SC Bu-TDPP films than in the case of the powder Bu-TDPPs. In Fig. 3, we observe 3 prominent polar modes at 35, 55 and 66 cm^{-1}, and a not well pronounced modulation in the range of 13–17 cm^{-1}. The distinct mode at 35 cm^{-1} corresponds to the M7 mode with A_u symmetry listed in Table 1. The weak feature

Table 1 Gamma-point frequencies ω (cm^{-1}), their irreducible representations, and the approximate displacement of each molecule in the six lowest-lying vibrational modes of Bu-TDPP (lattice translations omitted). Modes investigated further are in bold. A visual representation for mode 2 (marked in red) is shown in Fig. 2. Axes x and y are in horizontal and vertical directions, respectively

#	ω	Irrep.	Description
M1	10.5	B_u	$+y$; $-y$; $-y$; $+y$
M2	15.6	A_u	$+x$; $-x$; $-x$; $+x$
M3	18.9	B_g	$+x$; $+x$; $-x$; $-x$
M4	22.2	A_g	$+x+y$; $-x+y$; $+x-y$; $-x-y$
M5	25.4	A_g	$+x-y$; $-x+y$; $+x-y$; $-x+y$
M6	29.6	B_g	$+y$; $-y$; $+y$; $-y$

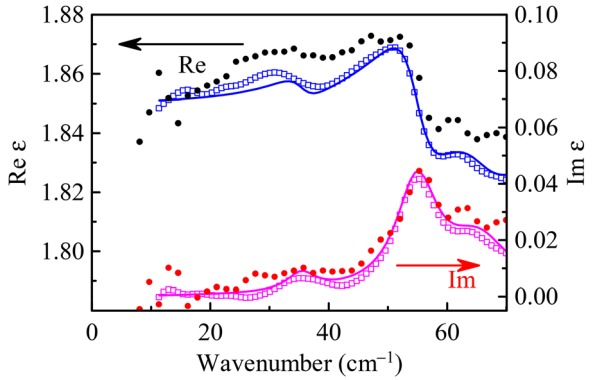

Fig. 3 THz spectra of the real and imaginary parts of the permittivity of the Bu-DPP powder in a 0.5 thick cuvette (black and red, full symbols) and in a 0.6 mm thick pressed pellet (blue and magenta, empty symbols). The permittivity of the pellet is significantly higher due to the higher density of the pressed sample (the values in the plot are multiplied by a factor of 0.6). Lines: fit of the data acquired on the pellet with a sum of 3 harmonic oscillators.

near 15 cm^{-1} can be related to the mode M2 A_u symmetry (Table 1) but the signal-to-noise ratio in this part of the spectrum is not high enough to enable an unambiguous determination of this weak mode.

2.2.3. Raman spectroscopy. Raman spectra of the Bu-TDPP obtained on the thin film cast on the Quartz substrate below 50 cm^{-1} are shown in Fig. 4. The wavelength of the incident light is 514.5 nm, which is close to one of the peaks in the steady state absorption spectrum (Fig. 1a). The Raman spectra are therefore recorded in the resonance mode, where vibrational modes coupled with the transition $|S_0, S_0\rangle \rightarrow |S^-\rangle$ are amplified. As the used laser cutoff filter starts to attenuate below 20 cm^{-1}, the data were corrected for its spectral characteristics to obtain the normalized intensity down do $\sim$7 cm^{-1}. Even though the compound is highly fluorescent when excited at 514.5 nm, the fluorescence did not obscure the signal in this low frequency region. There is a vibration mode at 19 cm^{-1} clearly seen in the figure. The shoulder at *ca.* 9 cm^{-1} is

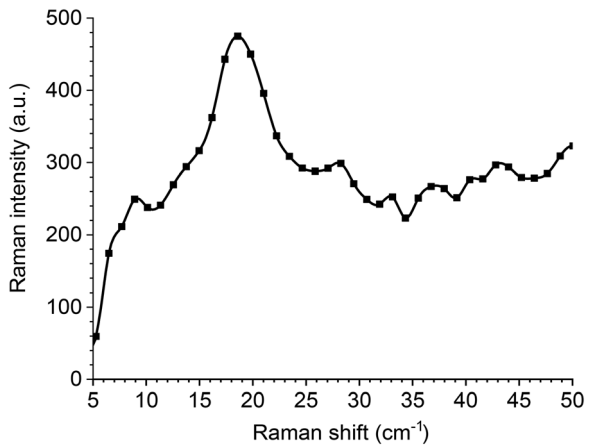

Fig. 4 Raman spectra of the Bu-TDPP thin film. Excitation wavelength: 514.5 nm.

less pronounced and is evidently on the edge of the spectrometer detection limit but both modes are well replicated in the anti-Stokes spectral region and seem to be real.

2.2.4. Vibrational mode distribution. Since the duration of the pump pulse (100 fs) is comparable to the timescale of an intramolecular energy redistribution and the reorganization energy is high (*vide supra*), the molecules are considerably heated upon photoexcitation and the subsequent transfer of energy towards low frequency inter-molecular modes is very fast, completed within several ps.[18,19] The redistributed reorganization energy of 0.18 eV is almost by two orders of magnitude higher than the energy quantum $\hbar\omega = 0.0025$ eV of the observed vibrational mode.

For the mean value of the quadratic displacement $\langle Q^2 \rangle$ of the low-frequency normal mode we find:

$$\langle Q^2(t) \rangle = \frac{1}{2}\mathrm{Tr}\left\{ \left(b e^{-i\omega t} + b^+ e^{i\omega t} \right)^2 \rho \right\} \xrightarrow{\frac{\hbar\omega}{k_B T} \to 0} \frac{k_B T}{\hbar\omega} + \frac{1}{2} + \frac{1}{2}\left(\langle b^2 \rangle e^{-i2\omega t} + \langle (b^+)^2 \rangle e^{i2\omega t} \right), \quad (9)$$

where b and b^+ are annihilation and creation operators of the considered vibrational mode, k_B is the Boltzmann constant and T is the local temperature.

As we know from the experiment, the term $\frac{k_B T}{\hbar\omega} \gtrsim 10$ means that the potential energy at the wings of the energy distribution $\left(\frac{\hbar\omega}{2} \langle Q^2(t) \rangle \approx \frac{k_B T}{2} + \frac{\hbar\omega}{4} \right)$ significantly exceeds that of a single vibrational quantum $\hbar\omega$ (Fig. 5) implying a very wide energy distribution of the low-frequency mode. We also note in eqn (9) the presence of time-dependent terms oscillating with the double frequency 2ω, which become active when the

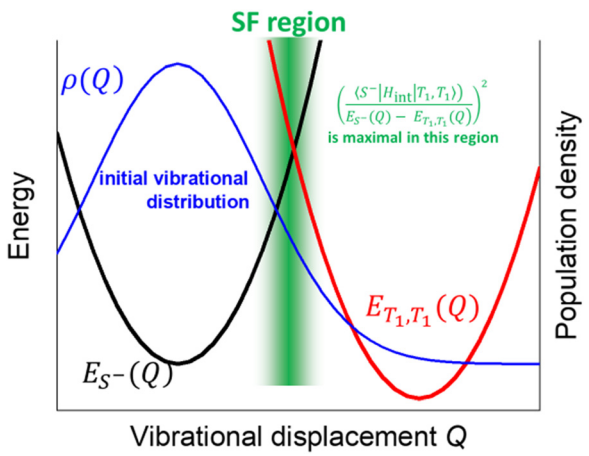

Fig. 5 The potential energy surfaces of singlet (black) and triplet pairs (red) and the population density distribution of vibration modes (blue). The region where the SF process takes place is marked by green. It is proportional to the overlap of $\left(\frac{\langle S^- | H_{int} | T_1, T_1 \rangle}{E_{S^-}(Q) - E_{T_1,T_1}(Q)} \right)^2$ and the vibrational distribution $\rho(Q)$. The latter is initially broad and breathing so that hot coherent population exchange between singlet and triplet pair occurs.

vibrational distribution is not thermalized and, at the same time, the conditions $\langle b^2\rangle \neq 0$, $\langle (b^+)^2\rangle \neq 0$ are fulfilled. The dominant contribution to such terms comes mainly from *the breathing of wide wings* of the unthermalized distribution. If the TA is driven by $\langle Q^2(t)\rangle$, the experimentally observed oscillations would have the frequency 2ω, *i.e.*, the modes around 10 cm^{-1} should be considered. In contrast, if the oscillations in the TA are driven by a coherent motion of the center of the wave-packet given by the mean displacement $\langle Q(t)\rangle \approx \frac{1}{\sqrt{2}}(\langle b\rangle e^{-i\omega t} + \langle b^+\rangle e^{i\omega t})$, the vibration mode at 20 cm^{-1} would be responsible for the modulation of the TA.

We also note that very wide distribution of the low-frequency intermolecular modes promotes the SF at the wings of the distribution because here the probability of the crossing of the potential energy surfaces (PES) between singlets (S) and triplet-pair (TT) states rapidly increases, as shown in Fig. 5. Here, the process of the SF takes place in the green region, where displaced potential energy surfaces of singlet and triplet pairs overlap. We note that as the initial thermal energy ($\geq$0.025 eV) is significantly higher than the energy quantum $\hbar\omega$ of low frequency intermolecular modes, the amplitudes of their oscillations are large. Consequently, the probability of approaching the conical intersection of the singlet and triplet-pair potential energy surfaces is high, too. Thus, the unthermalized vibrations should control the periodic oscillations found in the TA spectra during the SF process.

2.3. Vibrational modulation of TA spectra

The vibrational modulation of TA spectra can be explained either by vibrationally controlled population exchange between S and TT states, or by vibrationally controlled modulation of the transition dipole moments involved in the SF process, or also by impulsive stimulated Raman scattering (ISRS). Let us discuss these three possibilities in more detail.

2.3.1. Vibrational modulation of the population exchange of singlets and triplet pairs by low frequency modes. First, we can show that the singlet state is rather delocalized over two adjacent molecules forming a dimer, than localized on a single molecule.

Let us assume that the excited state $|S_1\rangle$ is fully localized on a single molecule of Bu-TDPP. Then, the GSB should correspond to the single molecule transition $|S_0\rangle \rightarrow |S_1\rangle$. In Fig. 1a, we see that very shortly after photoexcitation the difference TA spectrum between 480 nm and 600 nm is notably lower in absolute values than the GSB calculated from the pump fluence and the steady-state ground state absorption (cyan curve in Fig. 1a). It could be explained only if there is an additional ESA process $|S_1\rangle \rightarrow |S_m\rangle$ in the same spectral region that shifts the TA to more positive values.

For the excitation delocalized over two adjacent molecules, *i.e.* for the transition $|S_0, S_0\rangle \rightarrow |S^-\rangle$, it can be shown that it is redshifted and its oscillator strength is equal to twice the oscillator strength of a single molecule absorption $|S_0\rangle \rightarrow |S_1\rangle$ (eqn (S.II.4) in the SI). For the probe pulse, the transition $|S^-\rangle \rightarrow |S_1, S_1\rangle$ is also optically allowed and with twice the oscillator strength and blue-shifted compared to the single molecule absorption $|S_0\rangle \rightarrow |S_1\rangle$ (eqn (S.II.5)–(S.II.6) in the SI). It means that the transition $|S^-\rangle \rightarrow |S_1, S_1\rangle$ has the same oscillator strength as the transition $|S_0, S_0\rangle \rightarrow |S^-\rangle$, it is only partly blue-shifted. Thus, the ESA transition $|S^-\rangle \rightarrow |S_1, S_1\rangle$ can partly compensate the GSB.

As we also see in Fig. 1a, the two minima in TA at short times are more resolved and red-shifted compared to the GSB obtained from the steady state spectra. This can be achieved if the negative spectrum of the GSB is partly superimposed with its ''mirror'' picture (positive spectrum) but slightly blue-shifted. We can then expect that the singlet excitation is notably delocalized at least over two adjacent molecules.

The idea that the oscillations in TA signal can be explained by the vibrational modulation of the population exchange of S and TT states is supported by two experimental observations: first, by comparison of the ESA of singlet and triplet states and, second, by comparison of spectra of early time oscillations and the long-time asymptote in TA spectra.

2.3.1.1. Comparison of ESA of singlet and triplet states. Let us assume that the S state is delocalized inside a dimer. We can easily realize that both excited states $|S^-\rangle$ and $|T_1, T_1\rangle$ are equally shared by two molecules, which cannot participate in the absorption process $|S_0, S_0\rangle \rightarrow |S^-\rangle$ seen by the probe, so that both states equally contribute to the GSB. Then the population exchange between $|S^-\rangle$ and $|T_1, T_1\rangle$ can modulate the temporal evolution of the TA signal only by differences in their respective ESA spectra. The ESA of the state $|S^-\rangle$, observed between 480 and 600 nm, is given by the probe induced transition $|S^-\rangle \rightarrow |S_1, S_1\rangle$ which, except for a slight blue-shift by several nm due to the level splitting, provides a very similar spectrum as the absorption from the ground state, *i.e.*, $|S_0, S_0\rangle \rightarrow |S^-\rangle$. However, in Fig. 1a we see that the ESA of the singlet cannot fully compensate the GSB so that we conjecture that it can be approximated only by normalized steady-state absorption.

On the other hand, the ESA spectrum of the $|T_1, T_1\rangle$ state can be reconstructed from the long-time asymptote of the difference absorbance $\Delta A(\lambda, t \rightarrow \infty)$, the steady-state absorption and the experimentally determined yield f of the $|T_1, T_1\rangle$ state (see eqn (S.II.25) in the SI). Normalized ESA spectra of singlet and triplet-pair states are shown in Fig. 6a. We see that the ESA of the $|S^-\rangle$ state is notably higher at wavelengths between *ca.* 570 and 590 nm, while the ESA of the $|T_1, T_1\rangle$ is notably higher at wavelengths between *ca.* 490 and 510 nm. Both ESA spectra provide very similar values between *ca.* 520 and 560 nm. Thus, the increased TA at *ca.* 570–590 nm manifests an increased population of the $|S^-\rangle$ state, whereas the simultaneously decreased absorbance in the wavelength range of 490–510 nm points to a decreased population of the $|T_1, T_1\rangle$. The absorbance in the interval 520–560 nm practically remains unchanged. Then, the periodic population exchange between $|S^-\rangle$ and $|T_1, T_1\rangle$ states during short times will trigger the periodic antiphase oscillations in TA at *ca.* 490–510 nm and 570–590 nm, respectively.

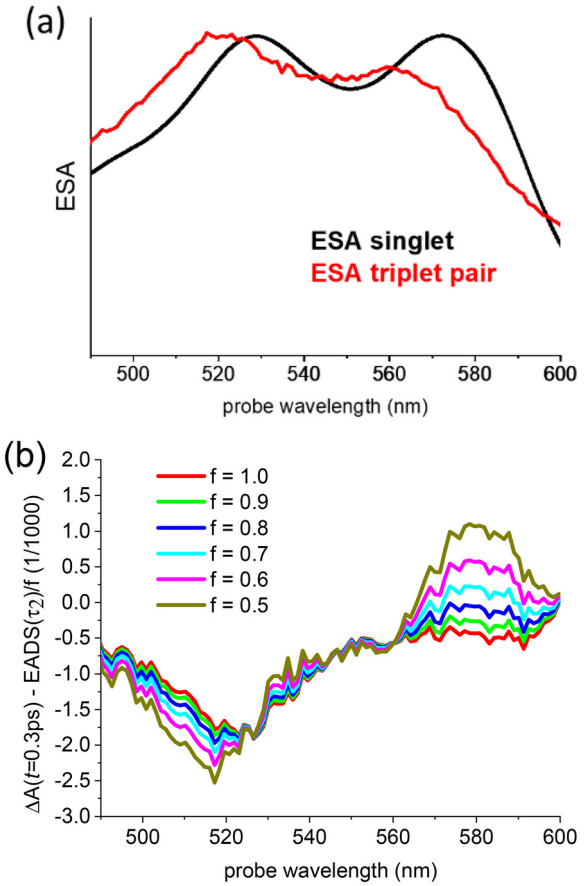

Fig. 6 (a) Normalized ESA spectra of singlet $|S^-\rangle \rightarrow |S_1, S_1\rangle$ and triplet pair states $|T_1, T_1\rangle \rightarrow |T_1, T_n\rangle$: the ESA of the singlet is proportional to the steady-state absorption (in the dimer model). The ESA of the triplet pair is obtained from the long-time TA, steady-state absorption and the SF yield published previously.[9] (b) Differences between ESA spectra of singlet and triplet states taken from TA experimental data calculated for various yield f of triplet pairs. The singlet ESA is taken from the short-time limit (eqn (10)), while the triplet pair ESA is taken from the long-time limit (eqn (11)).

We can come to the same conjecture, when ESA of the singlet is alternatively determined from the TA in the short-time limit. Thus, for the wavelengths range between 480 nm and 600 nm, we can describe the difference absorbance spectra at short- and long-time limits by the following relationships:

$$\Delta A(t \rightarrow 0, \lambda) \approx A_{|S^-\rangle \rightarrow |S_1, S_1\rangle}(\lambda) - A_{|S_0, S_0\rangle \rightarrow |S^-\rangle}(\lambda), \quad (10)$$

$$\Delta A(t \rightarrow \infty, \lambda) \approx f\left(A_{|T_1, T_1\rangle \rightarrow |T_1, T_n\rangle}(\lambda) - A_{|S_0, S_0\rangle \rightarrow |S^-\rangle}(\lambda)\right). \quad (11)$$

While eqn (10) assumes that at early times the TA is fully given by the absorption of the excited state $|S^-\rangle$, eqn (11) shows that the long-time limit of TA is fully controlled by triplet-pairs that are generated with the yield f. Just by subtracting these two equations, we can directly obtain the difference between ESA spectra of the $|S^-\rangle$ and $|T_1, T_1\rangle$ states as

$$A_{|S^-\rangle \rightarrow |S_1, S_1\rangle}(\lambda) - A_{|T_1, T_1\rangle \rightarrow |T_1, T_n\rangle}(\lambda) = \Delta A(t \rightarrow 0, \lambda) - \Delta A(t \rightarrow \infty, \lambda)/f. \quad (12)$$

In Fig. 6b, we show the experimentally determined difference spectra $\Delta A(\lambda, t = 0.3\ \text{ps}) - \text{EADS}(\lambda, \tau_2)/f$, corresponding to the right-hand-side of eqn (12), for various yield f of the of the TT pairs. Note that we see that the "anti-phase" intervals 500–530 nm and 560–600 nm in both Fig. 1b and in Fig. 6b can be easily distinguished.

2.3.1.2. Comparison of TA spectra of residuals of early time oscillations and the long-time asymptote. As an ideal limit of the model, we will now assume that the evolution of the TA spectra is driven only by the population transfer between $|S^-\rangle$ and $|T_1, T_1\rangle$, with the total population conserved ($P_S(t) + P_{TT}(t) = 1$). We will also assume an ideal dimer model, in which $A_{|S^-\rangle \rightarrow |S_1, S_1\rangle}(\lambda) \approx A_{|S_0, S_0\rangle \rightarrow |S^-\rangle}(\lambda)$, and the spectrum $A_{|S^-\rangle \rightarrow |S_0, S_n\rangle}(\lambda)$ in the interval 500–600 nm can be neglected. It can be shown (see derivation of eqn (S.II.26) in the SI) that the residuals of oscillations of the time course of the TA around their mean value, *i.e.*, $\text{Res}\{\Delta A(\lambda,t)\}$, are proportional to a product of the displacements of the singlet population $\left(P_S(t) - \overline{\langle P_S(t)\rangle}\right)$ and to the long-time asymptote of the differential spectrum $\Delta A(\lambda, t \rightarrow \infty)$ as follows

$$\begin{aligned} \text{Res}\{\Delta A(\lambda, t)\} &\equiv \Delta A(\lambda, t) - \overline{\langle \Delta A(\lambda, t)\rangle} \\ &\approx -\left(P_S(t) - \overline{\langle P_S(t)\rangle}\right)\frac{\Delta A(\lambda, t \rightarrow \infty)}{f} \end{aligned} \quad (13)$$

In eqn (13), the symbol $\overline{\langle \ldots \rangle}$ means averaging over a period of oscillations, so that the spectral variables $X(\lambda, t) - \overline{\langle x(\lambda, t)\rangle}$ (residuals) provide the local displacements due to the oscillations. In Fig. 1b, we see a perfect overlap of experimental data of the residuals of the short-time oscillation spectrum $\text{Res}\{\Delta A(\lambda,t)\}$ (blue and green vertical bars) and the long-time differential spectrum $\Delta A(\lambda, t \rightarrow \infty)$ (red line) as given by eqn (13).

2.3.2. Explicit modulation of transition dipole moments by vibrations. In the second model, which is based on the modulation of transition dipole moments by vibrations, we will discuss two limiting cases: (i) modulated localized excitation (vibronic model) and (ii) the excitonic model.

2.3.2.1. Vibronic model. The ESA spectra can be influenced by transition dipole moments varied by interacting vibronic transitions. The pump and probe pulse have a finite duration ($\tau_p \approx 100$ fs), consequently, the contribution of various vibrational modes depends on their frequency. We can distinguish two limit cases:

For very fast vibration modes, $\omega\tau_p \gg 1$ (stationary excitation). The vibronic levels are populated on a shorter timescale than the pulse duration, thus the obtained spectra correspond to the stationary absorption (see Chapter 5.3. of ref. 25 or Section SIII in the SI). Namely, we remind in this context the above-discussed strong vibronic FC transitions with the energy separation of 0.18 eV (1450 cm^{-1}) between FC peaks. For such fast modes with a period of 22 fs, the duration of the probe pulse of *ca.* 100 fs is almost stationary, and the absorption spectrum nearly follows the steady state absorption, not changing with the time delay t between pump and probe. Hence, such modes cannot be recognized in time-resolved TA,

however, if they notably contribute to the reorganization energy, which can enhance the SF, their FC factors could be seen in the steady state absorption spectra.

For very slow vibration modes, $\omega\tau_p \ll 1$ (pulse excitation). The modes are quasi-static on the timescale of the optical pulses. The density matrix of such modes is unchanged during the absorption process so that they will not contribute to the wavelength dependence of the ESA spectra (see eqn. (5.3.21) in ref. 25). This is the case of sub-THz modes which might be responsible for the oscillations in the TA spectra.

We can then factorize the density matrix of the excited state into a product of distributions of vibronic (electronic + high frequency modes) and low frequency modes (see Chapter 5.3 of ref. 25). When the probe enters the system, we can also factorize the oscillator strength of the transition $|S^-, m\rangle \rightarrow |S_1, S_1, n\rangle$ to the form $\langle m_{S^-} \mid n_{S_1,S_1}\rangle_{fast}^2 \cdot \left\langle d_{S^-;S_1,S_1}(Q(t))^2 \right\rangle_{slow} R_g(Q(t))$, where $R_g(Q(t))$ is the distribution of inter-molecular modes. While the Franck–Condon term $\langle m_{S^-} \mid n_{S_1,S_1}\rangle_{fast}^2$ is formed by the fast vibronic modes and becomes only wavelength-dependent, in contrast, the term $\langle d_{S^-;S_1,S_1}(Q(t))^2\rangle_{slow}$ reacts to the instant position of slow modes and becomes only time-dependent. Then, if slow modes would modulate the transition dipole moment $d_{S^-;S_1,S_1}(Q(t))$, their modulation of the ESA spectra should be independent on the probe wavelength and thus uniform over the investigated spectral range. Consequently, the modulation of transition dipole moments by slow modes cannot contribute to the antiphase oscillations in the intervals 480–520 nm and 520–560 nm in Fig. 1b.

2.3.2.2. Excitonic model. Let us now assume the case of a Frenkel exciton without the vibrational dressing. The corresponding ESA of the momentum dependent transition $|S(k)\rangle \rightarrow |S_1, S_1\rangle$, will be similar to the ground state absorption spectrum, *i.e.*, the transition $|S_0\rangle \rightarrow |S(k)\rangle$. The results of such calculation are shown in Fig. S1 and S2 in the SI. The coupling between vibrational modes M1–M3 and electronic transitions were investigated computationally by modulating the Bu-TDPP geometry along these modes and evaluating the changes caused by the displacement. In all cases, we found that the change in the absorption spectra only depends on the magnitude of the displacement, *i.e.*, same changes were observed when modulating the geometry in the (+) and (–) direction. Therefore, the exciton delocalization can modulate the oscillatory pattern of the TA only by terms $\exp(\pm i2\omega t)$.

Results are shown for the movement along the M2 mode, which was shown to produce the largest changes in the absorption intensity (>20%), while results for M1 and M3 provided smaller changes (below 10% and 5%, respectively) (see Fig. S1 and S2 in the SI). The calculated absorption spectrum of Bu-TDPP in Fig. S2 shows two peaks at ~566 nm and ~505 nm associated with the HOMO–LUMO absorption, which quantitatively correspond to experimental peaks at 580 and 500 nm in Fig. 1. We note that the displacement along the M2 mode results in the antiphase modulation of the absorption spectra transition moment at ~566 nm and ~505 nm. We see that for the vibrational geometry different from the equilibrium position the intensity of the absorption increases at *ca.* 2.46 eV (505 nm), while at *ca.* 2.19 eV (566 nm), the intensity of the absorption decreases. We see in Fig. 1c that immediately after the photoexcitation, the TA evolves in this way at *ca.* 505 nm and 581 nm. This would mean that immediately after the photoexcitation, the inter-molecular modes should be in the equilibrium position. However, if they were in equilibrium, they would not be able to oscillate. Oppositely, after the pump pulse the inter-molecular modes are not in equilibrium for two reasons:

First, during the interaction with a pump pulse with a duration of *ca.* 100 fs, high frequency modes relax to their new position ($\langle q\rangle \neq 0$). The Duschinsky bilinear coupling between intra-molecular and inter-molecular modes, which is proportional to qQ, is then added to the potential $\hbar\omega\frac{Q^2}{2}$ of the inter-molecular modes. This will cause a shift of the equilibrium position of the inter-molecular mode.

Second, if the transition dipole moment $d_{G,S(k)}(Q)$ of the transition $|G\rangle \rightarrow |S(k)\rangle$ is dependent on Q, then the equilibrium vibrational distribution $R_G(Q)$ in the ground state before photoexcitation is changed after the impact of the pump pulse to a new nonequilibrium distribution proportional to $d^2_{G,S(k)}(Q)R_G(Q)$.

We thus conjecture that if the population exchange between singlet and triplet states is omitted from the excitation dynamic, the vibration modulation of the transition dipole moments by slow vibrational modes cannot explain the time-resolved oscillations in the TA spectra by either the localized (vibronic) or excitonic model.

2.3.3. Ground state bleach modulation by the impulsive stimulated Raman scattering. When the excitation pump pulse wavelength approaches the wavelength of the transition $|S_0, S_0\rangle \rightarrow |S^-\rangle$, it may notably enhance the Raman scattering. Due to the finite duration of *ca.* 100 fs of the pump pulse, the latter process can create a vibrational coherent state in the ground state. After the impact of a probe pulse, molecules with Raman-induced vibrational coherence can undergo the transition $|S_0, S_0\rangle \rightarrow |S^-\rangle$. This can potentially create vibrational residuals in the differential TA spectra, as they subtract absorption of the vibrationally excited ground state and the steady state absorption.

The duration of the pulse of $\tau_p \approx 100$ fs also brings an energy width of the pulse $\Delta E \geq 3.3$ meV $\left(\Delta E\tau_p \geq \frac{\hbar}{2}\right)$. This value is enough to excite a coherent state for the mode with the vibrational quantum 2.5 meV (20 cm^{-1}). On the other hand, for the room temperature at *ca.* 300 K, the thermal energy is 25 meV, which is an order of magnitude more than the energy width ΔE of the pulse. In fact, we observe a huge dispersion of the vibrational displacement (see eqn (9)). Therefore, the vibrational displacement in the ground state is strongly randomized, which also corresponds to a randomized phase of oscillations spread over a total period of *ca.* 1.6 ps. Secondly, there is also no reason why the probe at wavelengths of *ca.* 505 and 580 nm should bring these antiphase oscillations.

We thus conjecture that vibrational oscillations in TA spectra cannot be explained by the Raman-induced vibrational coherence in the ground state.

2.3.4. Effects near the conical intersection between potentials of singlets and triplet pair states. Even if the vibrationally-controlled transition dipole moments cannot explicitly explain the oscillatory pattern in the TA, they can be important implicitly for both the SF process and for early time oscillations in the time course of the TA. Namely, the energy of the dimer state $|S^-\rangle$ is notably controlled by the dipole–dipole interaction of the transition dipole moments (*cf.* eqn (S.II.1)–(S.II.3) in the SI) between respective molecules. Hence, the inter-molecular vibrations modulating the transition dipole moments will also contribute to the shift of the energy and to the equilibrium position of the dimer state $|S^-\rangle$ (eqn (S.II.3) in the SI), modifying thus the energy detuning $\Delta\varepsilon(Q) \equiv E_{S^-}(Q) - E_{T_1,T_1}(Q) \to 0$ in eqn (5). Assuming the central symmetry for the dimer state, we also easily find for the equilibrium position in the ground state that $\langle S^-|H_{int}|T_1,T_1\rangle(Q \to 0) \to 0$ (*cf.* eqn (S.II.17)). As the inter-molecular vibrations break the symmetry, the SF coupling energy becomes $\langle S^-|H_{int}|T_1,T_1\rangle(Q) \sim Q$ (*cf.* eqn. (S.II.17)), *i.e.*, proportional to the vibrational displacement Q. The adiabatically dependent populations of $|S^-\rangle$ and $|T_1,T_1\rangle$ states are controlled by even powers of $\{\tan(2\alpha)\}^{2n}(Q) = \left\{\frac{2\langle S^-|H_{int}|T_1,T_1\rangle}{\Delta\varepsilon(Q)}\right\}^{2n}$ (eqn (S.II.10)–(S.II.11) in the SI). Then, the populations of $|S^-\rangle$ and $|T_1,T_1\rangle$ states are in the statistical ensemble controlled by the terms proportional to $\left\langle\left(\frac{Q}{\Delta\varepsilon(Q)}\right)^{2n}(t)\right\rangle$. We note that the "energy resonance" denominator term $\Delta\varepsilon(Q)$ significantly enhances contributions to the population exchange from the regions where respective PESs intersect or approach (see Fig. 5), *i.e.*, when $\Delta(Q) \to 0$ and $E_{S^-}(Q) \to E_{T_1,T_1}(Q)$. Moreover, near the PES intersection the time-dependent part of $\left\langle\tan(2\alpha)^2(Q(t))\right\rangle \sim \left\langle\left(\frac{Q}{\Delta\varepsilon(Q)}\right)^2(t)\right\rangle$ converges to $\frac{\langle b^2\rangle e^{-i2\omega t} + \langle(b^+)^2\rangle e^{i2\omega t}}{\{\Delta\varepsilon(Q)\}^2}$. This means that the enhanced population transfer between S and TT states becomes controlled, to the lowest order, by the doubled frequency 2ω of the mode.

Now we answer the following key point: how to relate the short time (heated oscillations) with the irreversible (perturbative) process? In the coherent regime, the mixing parameter can be factorized as

$$\left\langle\tan(2\alpha)^2(Q(t))\right\rangle = 4\left(\frac{\partial\langle S^-|H_{int}|T_1,T_1\rangle}{\partial Q}\right)^2\left\langle\left(\frac{Q}{\Delta\varepsilon(Q)}\right)^2(t)\right\rangle \quad (14)$$

Thus, in the coherent regime, the time-dependent part $\left\langle\left(\frac{Q}{\Delta\varepsilon(Q)}\right)^2(t)\right\rangle$ can be resonantly enhanced as discussed above. However, we also note the prefactor $4\left(\frac{\partial\langle S^-|H_{int}|T_1,T_1\rangle}{\partial Q}\right)^2$. In the thermalized regime, the vibrational displacement $Q(t)$ approaches its equilibrium position Q_e and the mixing parameter $\left\langle\tan(2\alpha)^2(Q(t))\right\rangle$ becomes small and the system undergoes a perturbative transition to the TT states. The rate r of this transfer is given by the Fermi Golden Rule

$$r = \frac{2\pi}{\hbar}|\langle S^-|H_{int}(Q_e)|T_1,T_1\rangle|^2\delta(\Delta\varepsilon(Q_e)) \to$$
$$\to 2|\langle S^-|H_{int}(Q_e)|T_1,T_1\rangle|^2\frac{k}{\left((\Delta\varepsilon(Q_e))^2+(\hbar k)^2\right)} \to$$
$$2\left(\frac{\langle S^-|H_{int}(Q_e)|T_1,T_1\rangle}{\Delta\varepsilon(Q_e)}\right)^2 k \approx 2\left(\frac{\partial\langle S^-|\partial H_{int}|T_1,T_1\rangle}{\partial Q}\right)^2\left\langle\frac{Q_e^2}{\Delta\varepsilon(Q_e)}\right\rangle k \quad (15)$$

In eqn (15) we approximated the delta-function by the Lorentzian distributions, with the line width controlled by the rate of the vibrational dephasing k, which is weaker than the energy detuning $\Delta\varepsilon(Q_e)$ between the S and TT states, *i.e.*, $\hbar k \ll |\Delta\varepsilon(Q_e)|$. In eqn (15) we can find several important consequences. First, the term $4\left(\frac{\langle S^-|H_{int}(Q_e)|T_1,T_1\rangle}{\Delta\varepsilon(Q_e)}\right)^2$ was shown in the SI (see eqn (S.II.14) and the discussion after it) to correspond to the maximum probability transfer from S to TT states in the case of static and weak perturbative limits of the dimer model. Thus, the rate r can be interpreted as the "mean" probability transfer between the S and TT states inside the dimer model multiplied by the rate of the vibrational dephasing. Secondly, as in the perturbative regime the fraction $2\left(\frac{\langle S^-|H_{int}(Q_e)|T_1,T_1\rangle}{\Delta\varepsilon(Q_e)}\right)^2 \ll 1$, then also for the rate r, we find $r \ll k$, *i.e.*, the rate of the formation of the TT states by the vibrational coupling must occur on (much) longer time frames, then the rate k of vibrational dephasing. For the third, we explicitly see that both mixing parameter $\left\langle\tan(2\alpha)^2(Q(t))\right\rangle$, which controls oscillations in TA spectra at early times, and the rate r are proportional to the same prefactor $\left(\frac{\partial\langle S^-|H_{int}|T_1,T_1\rangle}{\partial Q}\right)^2$. The last one arises due to the explicit dependence of the term $\langle S^-|H_{int}|T_1,T_1\rangle$ on the vibrational displacement Q.

3. Conclusion

From the analysis of the transient absorption spectra of thin films of derivatives of diketopyrrolopyrroles carrying *n*-hexyl, *n*-butyl, or 2-(adamant-1-yl)ethyl substituents, we conclude:

– The singlet fission yields over 100% are always accompanied with clearly resolved oscillations at short times after photoexcitation with a period on the ps time scale.

– The most clearly resolved oscillations with a period of 1.6 ps (20 cm^{-1}) were found in the transient absorption spectra of spin-coated thin solid films of 3,6-bis(2-thienyl)-2,5-bis(butyl)-2,5-dihydro-pyrrolo[3,4-*c*]pyrrole-1,4-dione (Bu-TDPP), with a SF yield of about 160%.

– Contrary to our previous publication,[9] where the singlet fission process was explained only by interactions of delocalized excitons interacting with triplet-pair states *via* intermediate charge transfer states, we propose a different model, which explains the oscillations observed in transient absorption by the population exchange between singlets and triplet-pairs states localized on adjacent molecules closely packed in a centrosymmetric configuration. This population exchange is driven by their low-frequency intermolecular vibrational modes.

– We show that for the system in the centrosymmetric configuration, the matrix element of the coupling between the singlet and triplet states increases with the displacement of these inter-molecular modes. The vibration-induced oscillations in the populations of singlets and triplet pair state at the ps time scale are correlated with the irreversible population transfer from the singlet state to the triplet-pair state that occurs later, at time scales of approximately 100 ps. The rate of this transfer is, in principle, always much slower than the rate of the vibrational dephasing.

– Very broad distribution of low-frequency modes results in efficient crossing of the potential energy surfaces between singlets and triplet-pair states, making the singlet fission more efficient.

– By means of the quantum chemistry, six inter-molecular modes in the 10–30 cm^{-1} range with symmetry against + and – inversion were found and confirmed by the Raman and THz spectroscopies.

– We confirmed that the explicit dependence of transition dipole moments on the inter-molecular modes cannot explain the observed oscillations in TA spectra.

4. Experimental and methods

Materials

Synthesis, preparation and characterization details of the thin solid films 3,6-bis(2-thienyl)-2,5-bis(butyl)-2,5-dihydro-pyrrolo[3,4-c]pyrrole-1,4-dione (Bu-TDPP) prepared by the spin-coating (SC) have been already published elsewhere.[26]

Time-resolved (pump–probe) absorption spectroscopy

The data were taken from our previous work, where the measurements were performed using a HELIOS instrument (Ultrafast Systems, LLC., USA) equipped with a Ti:sapphire regenerative amplifier (model Legend Elite from Coherent, Inc., USA), which was used for the generation of ultrashort pulses (<20 fs FWHM). Spectrally narrow excitation (pump) pulses were generated with a tunable optical parametric amplifier (model TOPAS-C from Light Conversion, Lithuania). Spectrally broadband (white-light continuum) probe pulses were derived from Ti:sapphire laser pulses by means of a CaF_2 single crystal. The experimental setup is described in detail in ref. 27.

THz spectroscopy was performed *via* a time-domain experiment. A custom setup was used, in which the experiment was driven by the femtosecond laser oscillator MIRA (800 nm, 50–80 fs, 76 MHz). Coherent THz pulses were generated in an interdigitated biased photoconducting antenna (TeraSED), and phase-sensitive detection was accomplished *via* electro-optic sampling in a ⟨110⟩-oriented ZnTe crystal. The spectral range spanned from ~0.2 THz to ~3.0 THz. The measurements were first taken on the Bu-TDPP powder in a 0.5 mm thick cuvette and compared to the THz spectra acquired on the 0.6 mm thick pressed pellet squeezed between two sapphire windows. The latter arrangement was more favorable for the lower frequency range, due to the possibility of a longer scan without artefacts originating from interface reflections. An attempt to measure the time resolved THz spectra using pump and probe techniques was also made on the same thin film samples as measured in the TA, in order to observe the development of the vibration modes upon photoexcitation. Unfortunately, due to the small thickness of the samples, which were much thinner than the wavelength of the used radiation (less than $\lambda/300$), no signal was detected.

Raman spectra were acquired on thin films cast on quartz substrates, the same as for the TA spectroscopy, using an RM-1000 RENISHAW Raman spectrometer equipped with a Bragg filter. The excitation wavelength was 514.5 nm, and the laser power was reduced to ~ 0.5 mW to minimize local heating. The acquisition time was 10 s.

Quantum chemical calculations

Periodic calculations were carried out using the VASP code[28] and the PAW method.[29] The experimental crystal structure[9] of Bu-TDPP was optimized with the rev-vdW-DF2[30] functional. To avoid Pulay stress, a relatively large planewave cutoff of 700 eV was used. Reciprocal space was sampled using a gamma-centered 2 × 2 × 2 grid, with *k*-points at the center and the edges of the Brillouin zone. A convergence criterion of 10^{-8} eV for the wavefunction and 10^{-6} eV $Å^{-1}$ for the Hellmann–Feynman forces was used. The optimization yielded a structure very similar to the experimental one, with a 1.6% average difference in the unit cell parameters.

Phonon calculations were carried out using phonopy.[31] Phonon frequencies were found to be positive across the entire Brillouin zone, confirming that the obtained geometry corresponds to a stable crystal phase (see the SI). IR and Raman spectra, as well as geometries modulated along normal modes were obtained using the Phonopy-spectroscopy code.[32]

When generating displaced geometries, anharmonicity was taken into account by sampling several points along the normal mode to determine the amount of displacement associated with an energy increase of 3.0 kcal mol^{-1} accurately. In all cases, displacements in both (+) and (–) directions were investigated. Partially self-consistent *GW* calculations (evGW_0)[33] were carried out by iterating only the quasiparticle energies until convergence better than 5 meV was reached, for which 4

iterations were required. A gamma-centered 2 × 2 × 2 grid was used. A denser grid was computationally beyond reach, but DFT calculations on grids up to 8 × 8 × 8 confirmed that the geometries and band energies were well converged at the 2 × 2 × 2 grid. Convergence tests showed that 4320 empty bands and a grid of 100 points on the imaginary frequency axis were sufficient to converge the QP gaps to better than 5 meV. Initial orbitals were determined using the PBE functional[34] and the 435 eV planewave cutoff. The response functions were evaluated using the 100 eV cut-off. Optical properties were evaluated using the Bethe–Salpeter equation (BSE) and included excitations associated with 24 occupied and 24 virtual orbitals (6 + 6 per molecule in the unit cell).

Author contributions

M Menšík was responsible for data analysis of the TA spectra, theoretical modelling, and the concept of the project. P. Toman was responsible for theoretical modelling. I. Roncevic and A. Zaykov carried out the quantum chemical calculations. P.Kužel carried out the THz spectra measurements and interpretation, while J. Pokorný carried out the Raman spectroscopy analysis and interpretation, D. Rais carried out TA measurements and data analysis, M. A. Thottappali carried out data analysis of the TA spectra and J. Pfleger was responsible for the project coordination. All authors contributed to the manuscript editing.

Conflicts of interest

There are no conflicts of interest to declare.

Data availability

The raw experimental and numerical data used to obtain the results presented in this manuscript are available from the corresponding author (e-mail: mensik@imc.cas.cz) upon reasonable request. Supplementary information (SI) is available. See DOI: https://doi.org/10.1039/d6cp01025c.

Acknowledgements

The support of the Czech Science Foundation, project No. 22-02005S, is greatly acknowledged.

References

1 A. A. Bakulin, S. E. Morgan, T. B. Kehoe, M. W. B. Wilson, A. W. Chin, D. Zigmantas, D. Egorova and A. Rao, Real-time observation of multiexcitonic states in ultrafast singlet fission using coherent 2D electronic spectroscopy, *Nat. Chem.*, 2016, **8**, 16–23.

2 A. J. Musser, M. Liebel, C. Schnedermann, T. Wende, T. B. Kehoe, A. Rao and P. Kukura, Evidence for conical intersection dynamics mediating ultrafast singlet exciton fission, *Nat. Phys.*, 2015, **11**, 352–357.

3 E. G. Fuemmeler, S. N. Sanders, A. B. Pun, E. Kumarasamy, T. Zeng, K. Miyata, M. L. Steigerwald, X. Y. Zhu, M. Y. Sfeir, L. M. Campos and N. Ananth, A direct mechanism of ultrafast intramolecular singlet fission in pentacene dimers, *ACS Cent. Sci.*, 2016, **2**, 316–324.

4 H. L. Stern, A. Cheminal, S. R. Yost, K. Broch, S. L. Bayliss, K. Chen, M. Tabachnyk, K. Thorley, N. Greenham, J. M. Hodgkiss, J. Anthony, M. Head-Gordon, A. J. Musser, A. Rao and R. H. Friend, Vibronically coherent ultrafast triplet-pair formation and subsequent thermally activated dissociation control efficient endothermic singlet fission, *Nat. Chem.*, 2017, **9**, 1205–1212.

5 K. Miyata, Y. Kurashige, K. Watanabe, T. Sugimoto, S. Takahashi, S. Tanaka, J. Takeya, T. Yanai and Y. Matsumoto, Coherent singlet fission activated by symmetry breaking, *Nat. Chem.*, 2017, **9**, 983–989.

6 N. R. Monahan, D. Sun, H. Tamura, K. W. Williams, B. Xu, Y. Zhong, B. Kumar, C. Nuckolls, A. R. Harutyunyan, G. Chen, H. L. Dai, D. Beljonne, Y. Rao and X. Y. Zhu, Dynamics of the triplet-pair state reveals the likely coexistence of coherent and incoherent singlet fission in crystalline hexacene, *Nat. Chem.*, 2017, **9**, 341–346.

7 C. Schnedermann, A. M. Alvertis, T. Wende, S. Lukman, J. Feng, F. A. Y. N. Schröder, D. H. P. Turban, J. Wu, N. D. M. Hine, N. C. Greenham, A. W. Chin, A. Rao, P. Kukura and A. J. Musser, A molecular movie of ultrafast singlet fission, *Nat. Commun.*, 2019, **10**, 1–11.

8 K. Miyata, F. S. Conrad-Burton, F. L. Geyer and X. Y. Zhu, Triplet Pair States in Singlet Fission, *Chem. Rev.*, 2019, **119**, 4261–4292.

9 D. Rais, P. Toman, J. Pfleger, U. Acharya, Y. R. Panthi, M. Menšík, A. Zhigunov, M. A. Thottappali, M. Vala, A. Marková, S. Stříteský, M. Weiter, M. Cigánek, J. Krajčovič, K. Pauk, A. Imramovský, A. Zaykov and J. Michl, Singlet Fission in Thin Solid Films of Bis(thienyl)diketopyrrolopyrroles, *ChemPlusChem*, 2020, **85**, 2689–2703.

10 H. G. Duan, A. Jha, X. Li, V. Tiwari, H. Ye, P. K. Nayak, X. L. Zhu, Z. Li, T. J. Martinez, M. Thorwart and R. J. Dwayne Miller, Intermolecular vibrations mediate ultrafast singlet fission, *Sci. Adv.*, 2020, **6**, 52–70.

11 W. Kim, N. A. Panjwani, K. C. Krishnapriya, K. Majumder, J. Dasgupta, R. Bittl, S. Patil and A. J. Musser, Heterogeneous singlet fission in a covalently linked pentacene dimer, *Cell Rep. Phys. Sci.*, 2024, **5**, 102045.

12 H. Seiler, M. Krynski, D. Zahn, S. Hammer, Y. W. Windsor, T. Vasileiadis, J. Pflaum, R. Ernstorfer, M. Rossi and H. Schwoerer, Nuclear dynamics of singlet exciton fission in pentacene single crystals, *Sci. Adv.*, 2021, **7**, 869–894.

13 S. L. Bayliss, L. R. Weiss, F. Kraffert, D. B. Granger, J. E. Anthony, J. Behrends and R. Bittl, Probing the Wave Function and Dynamics of the Quintet Multiexciton State with Coherent Control in a Singlet Fission Material, *Phys. Rev. X*, 2020, **10**, 021070.

14 A. Ashoka, N. Gauriot, A. V. Girija, N. Sawhney, A. J. Sneyd, K. Watanabe, T. Taniguchi, J. Sung, C. Schnedermann and

A. Rao, Direct observation of ultrafast singlet exciton fission in three dimensions, *Nat. Comm.*, 2022, **13**, 1–8.
15 S. Souri, D. Timmer, D. C. Lünemann, N. Hadilou, K. Winte, A. De Sio, M. Esmann, F. Curdt, M. Winklhofer, S. Anhäuser, M. Guerrini, A. M. Valencia, C. Cocchi, G. Witte and C. Lienau, Ultrafast Time-Domain Spectroscopy Reveals Coherent Vibronic Couplings upon Electronic Excitation in Crystalline Organic Thin Films, *J. Phys. Chem. Lett.*, 2024, **15**, 11170–11181.
16 J. K. Lynd and D. I. G. B. Raccah, Characterizing the Role of Peierls Vibrations in Singlet Fission with the Adaptive Hierarchy of Pure States, *J. Phys. Chem. Lett.*, 2025, **16**, 7273–7279.
17 I. Carmichael and G. L. Hug, Triplet–Triplet Absorption Spectra of Organic Molecules in Condensed Phases, *J. Phys. Chem. Ref. Data*, 1986, **15**, 1–250.
18 D. Rais, M. Menšík, B. Paruzel, D. Kurunthu and J. Pfleger, Phonons spreading from laser-heated gold nanoparticle array accelerate diffusion of excitons in an underlying polythiophene thin film, *Phys. Chem. Chem. Phys.*, 2017, **19**, 10562–10570.
19 G. V. Hartland, Optical Studies of Dynamics in Noble Metal Nanostructures, *Chem. Rev.*, 2011, **111**, 3858–3887.
20 M. Andrzejak, G. Mazur and P. Petelenz, Interpretational Pitfalls of Singlet Fission Studies by Impulsively Generated Vibrational Wavepackets, *J. Phys. Chem. C*, 2025, **129**, 12257–12267.
21 H. Marciniak, X. Q. Li, F. Würthner and S. Lochbrunner, One-dimensional exciton diffusion in perylene bisimide aggregates, *J. Phys. Chem. A*, 2011, **115**, 648–654.
22 E. Engel, K. Leo and M. Hoffmann, Ultrafast relaxation and exciton–exciton annihilation in PTCDA thin films at high excitation densities, *Chem. Phys.*, 2006, **325**, 170–177.
23 D. Rais, M. Menšík, B. Paruzel, P. Toman and J. Pfleger, Concept of the Time-Dependent Diffusion Coefficient of Polarons in Organic Semiconductors and Its Determination from Time-Resolved Spectroscopy, *J. Phys. Chem. C*, 2018, **122**, 22876–22883.
24 M. Menšík, D. Rais, M. A. Thottappali, P. Güloğlu, P. Toman, J. Vohlídal and J. Pfleger, Kinetics of the Photo-excited States in Thin Films of Metallo-Supramolecular Polymers With Ditopic Thiophene-Bridged Terpyridine Ligands, *Front. Chem.*, 2022, **9**, 766121.
25 V. May and O. Kühn, *Charge and Energy Transfer Dynamics in Molecular Systems*, Wiley-VCH Verlag GmbH, Berlin, Germany, 1st edn, 2000.
26 E. Zhou, Q. Wei, S. Yamakawa, Y. Zhang, K. Tajima, C. Yang and K. Hashimoto, Diketopyrrolopyrrole-Based Semiconducting Polymer for Photovoltaic Device with Photocurrent Response Wavelengths up to 1.1 μm, *Macromolecules*, 2009, **43**, 821–826.
27 D. Rais, J. Pfleger, M. Menšík, A. Zhigunov, P. Štenclová, J. Svoboda and J. Vohlídal, Singlet fission in thin films of metallo-supramolecular polymers with ditopic thiophene-bridged terpyridine ligands, *J. Mater. Chem. C*, 2017, **5**, 8041–8051.
28 G. Kresse and J. Furthmüller, Efficient iterative schemes for ab initio total-energy calculations using a plane-wave basis set, *Phys. Rev. B: Condens. Matter Mater. Phys.*, 1996, **54**, 11169.
29 P. E. Blöchl, Projector augmented-wave method, *Phys. Rev. B: Condens. Matter Mater. Phys.*, 1994, **50**, 17953.
30 I. Hamada, van der Waals density functional made accurate, *Phys. Rev. B: Condens. Matter Mater. Phys.*, 2014, **89**, 121103(R).
31 A. Togo and I. Tanaka, First principles phonon calculations in materials science, *Scr. Mater.*, 2015, **108**, 1–5.
32 J. M. Skelton, L. A. Burton, A. J. Jackson, F. Oba, S. C. Parker and A. Walsh, Lattice dynamics of the tin sulphides SnS2, SnS and Sn2S3: vibrational spectra and thermal transport, *Phys. Chem. Chem. Phys.*, 2017, **19**, 12452–12465.
33 M. Shishkin and G. Kresse, Implementation and performance of the frequency-dependent GW method within the PAW framework, *Phys. Rev. B: Condens. Matter Mater. Phys.*, 2006, **74**, 035101.
34 J. P. Perdew, K. Burke and M. Ernzerhof, Generalized Gradient Approximation Made Simple, *Phys. Rev. Lett.*, 1996, **77**, 3865.

